Supporting Information

Hierarchically hollow N-doped carbon-cobalt nanoparticle heterointerface for efficient bifunctional oxygen electrocatalysis

Xinyan Leng,[a] Cong Ling,[b] Xiao-Jie Lu,[b] Chenchen Qin,[a] Jian Zhang,[a] Jing-Han Li,[b] An-Wu Xu*[b] and Zhengkun Yang*[a]

[a]Institutes of Physical Science and Information Technology, Anhui Graphene Engineering Laboratory, Key Laboratory of Structure and Functional Regulation of Hybrid Materials (Anhui University), Ministry of Education, Hefei, 230601, China

[b]Hefei National Research Center for Physical Sciences at the Microscale, University of Science and Technology of China, Hefei, 230026, China.

*To whom correspondence should be addressed.

Email: anwuxu@ustc.edu.cn

yangzk@ustc.edu.cn

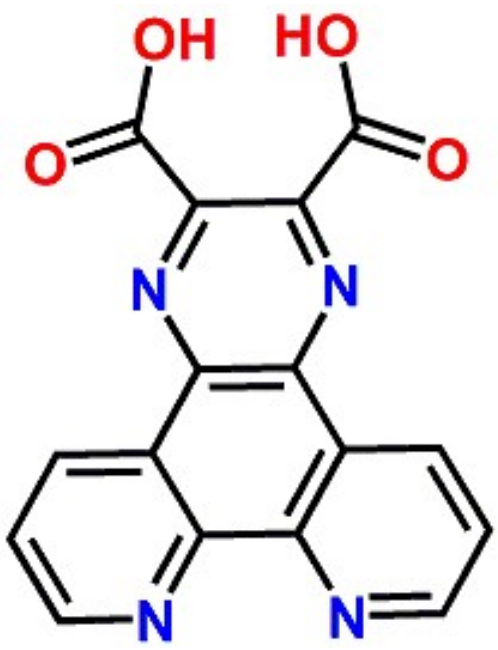

Figure S1. Molecular structure of H_2PPDA

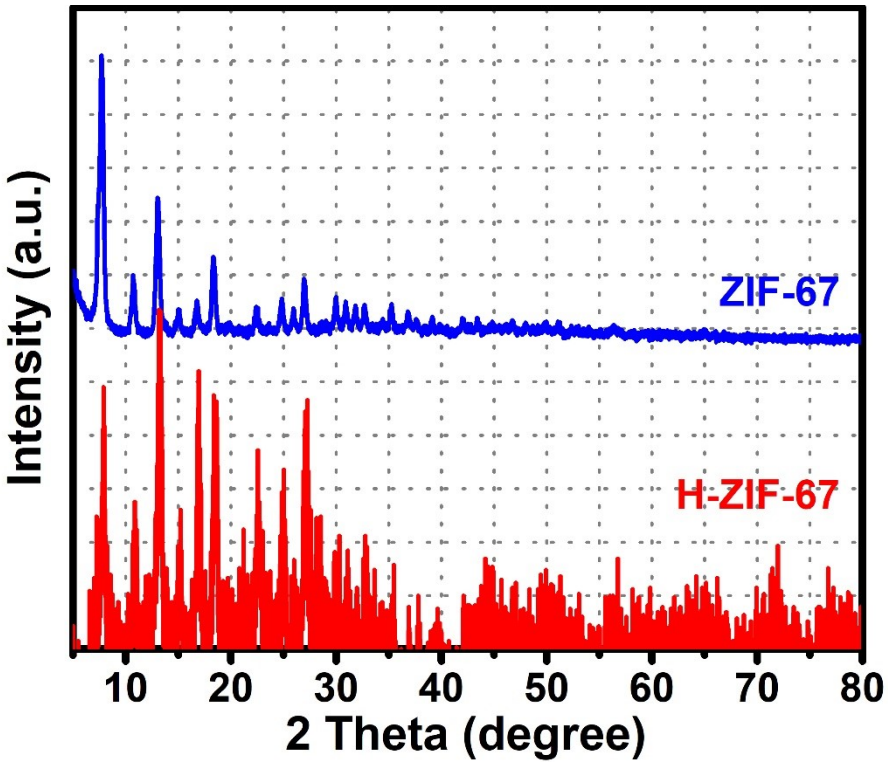

Figure S2. The XRD patterns of as-prepared ZIF-67 and H-ZIF-67 samples.

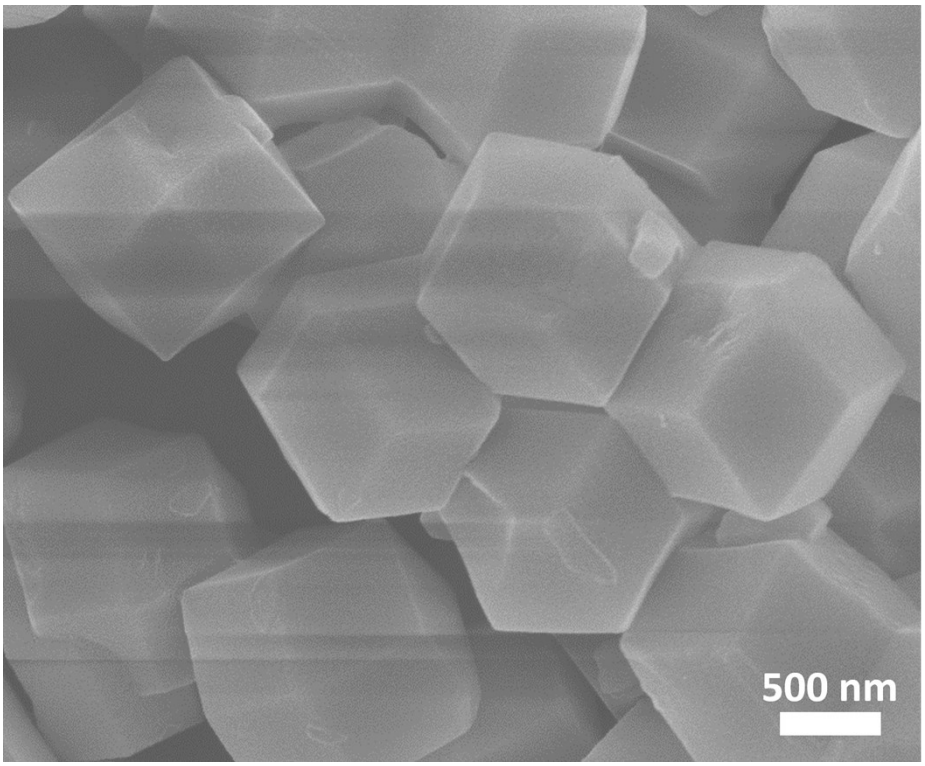

Figure S3. The SEM image of as-prepared ZIF-67 sample.

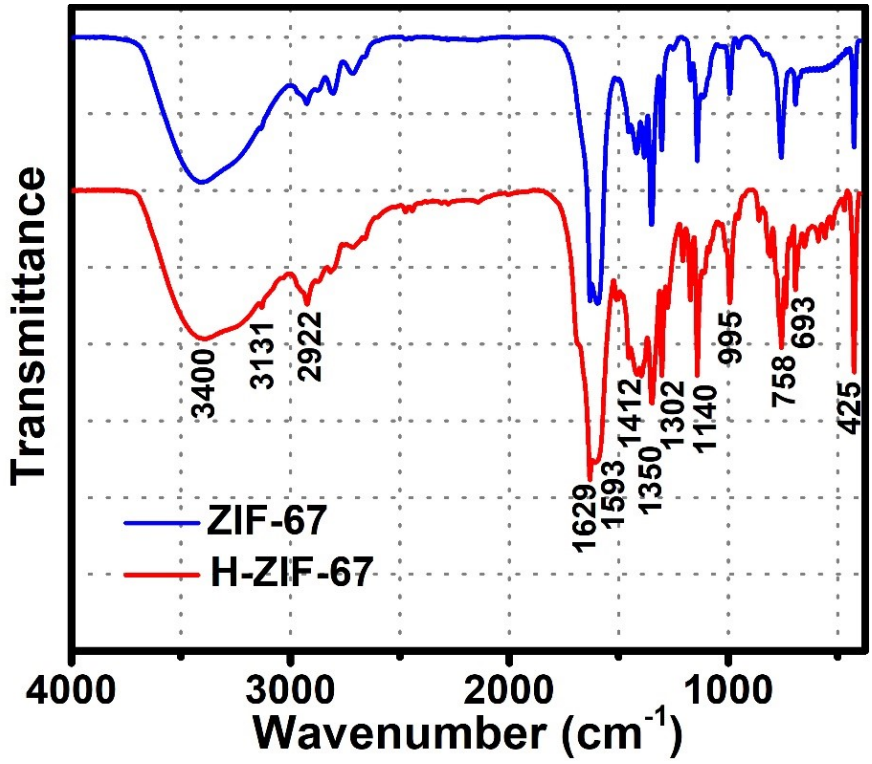

Figure S4. FTIR spectras of as-formed ZIF-67 and H-ZIF-67 samples.

The peak at 425 cm^{-1} is due to the Co-N vibrations. The bands at 693 and 753 cm^{-1} in

the spectral region are associated with out-of-plane bending of the imidazole ring, while peaks in the region of between 900 and 1350 cm^{-1} are assigned as in-plane bending. The peaks at 1593 and 1629 cm^{-1} are attributed to the stretching and bending N–H vibration of the imidazole ring, respectively. The intense and convoluted bands at 1350–1500 cm^{-1} are associated with the entire ring stretching, whereas two peaks at 2922 and 3131 cm^{-1} are attributed to the aliphatic and the aromatic C–H stretch of the imidazole, broad peak at 3400 cm^{-1} corresponds to the N-H stretching vibrations of 2-methylimidazole.

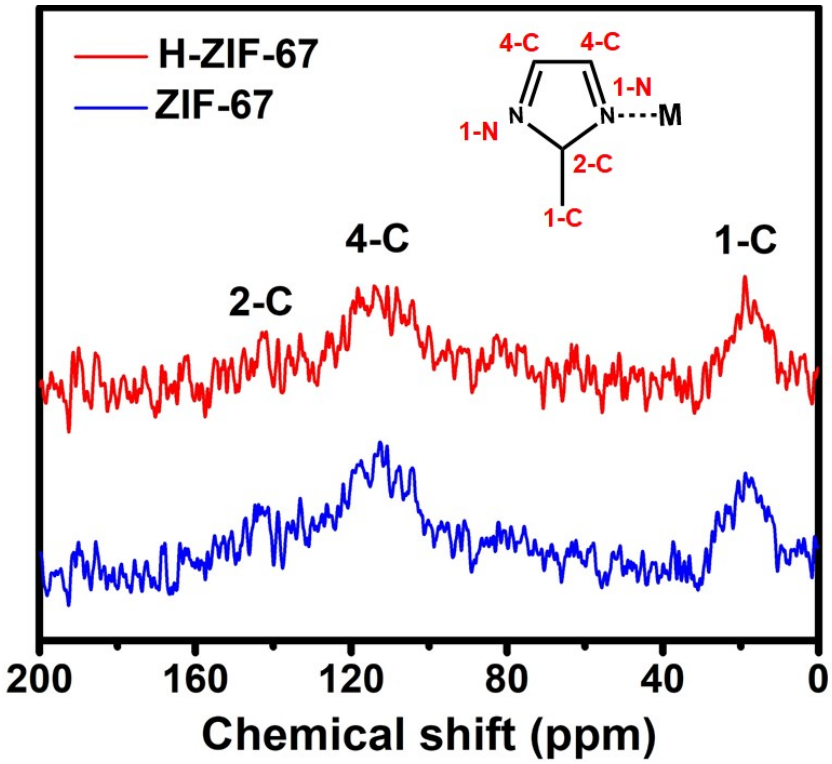

Figure S5. ^{13}C NMR spectra of ZIF-67 and H-ZIF-67 powders.

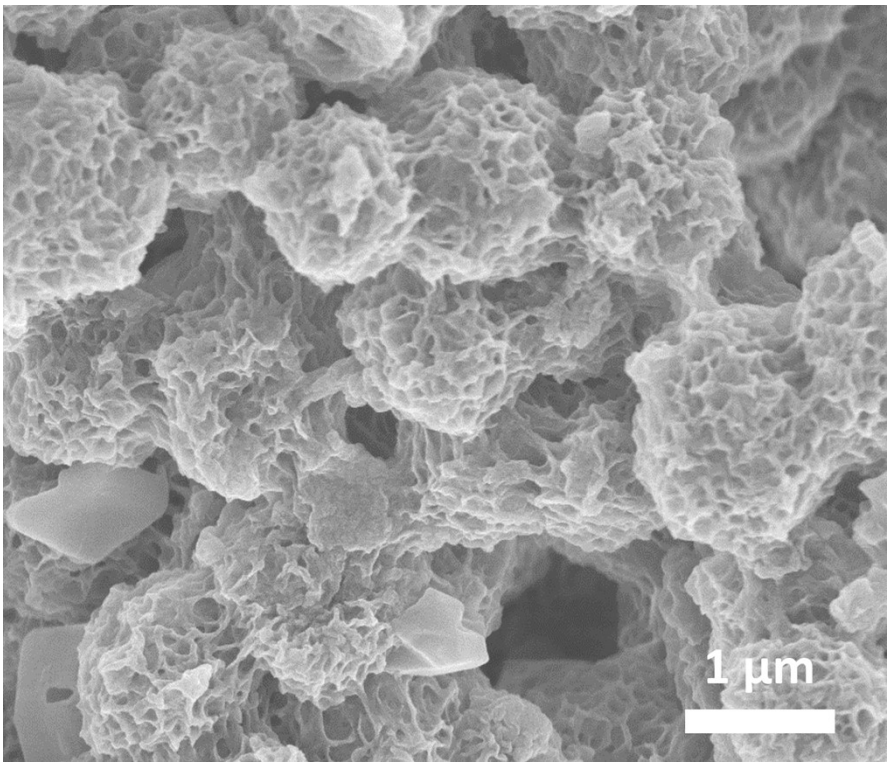

Figure S6. The SEM image of as-prepared H-ZIF-67 sample.

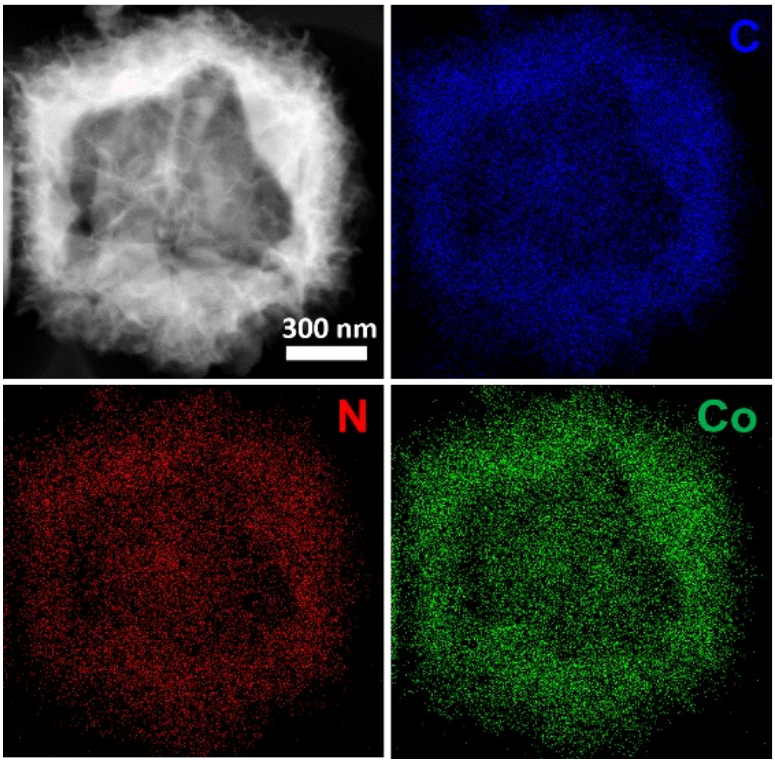

Figure S7. The EDS element mapping of as-prepared H-ZIF-67 sample.

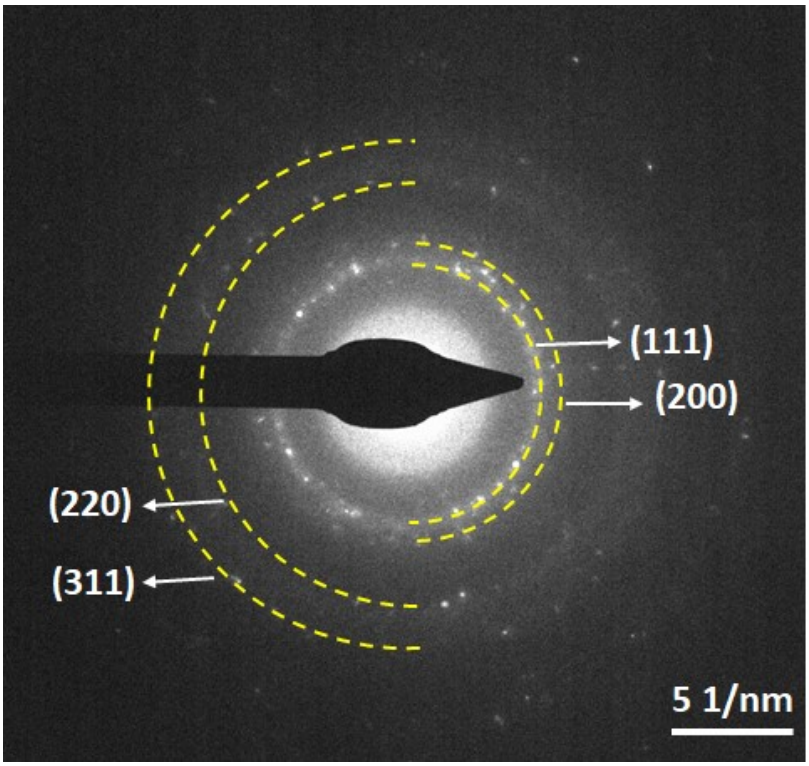

Figure S8. The selected area electron diffraction (SAED) pattern of a single cage.

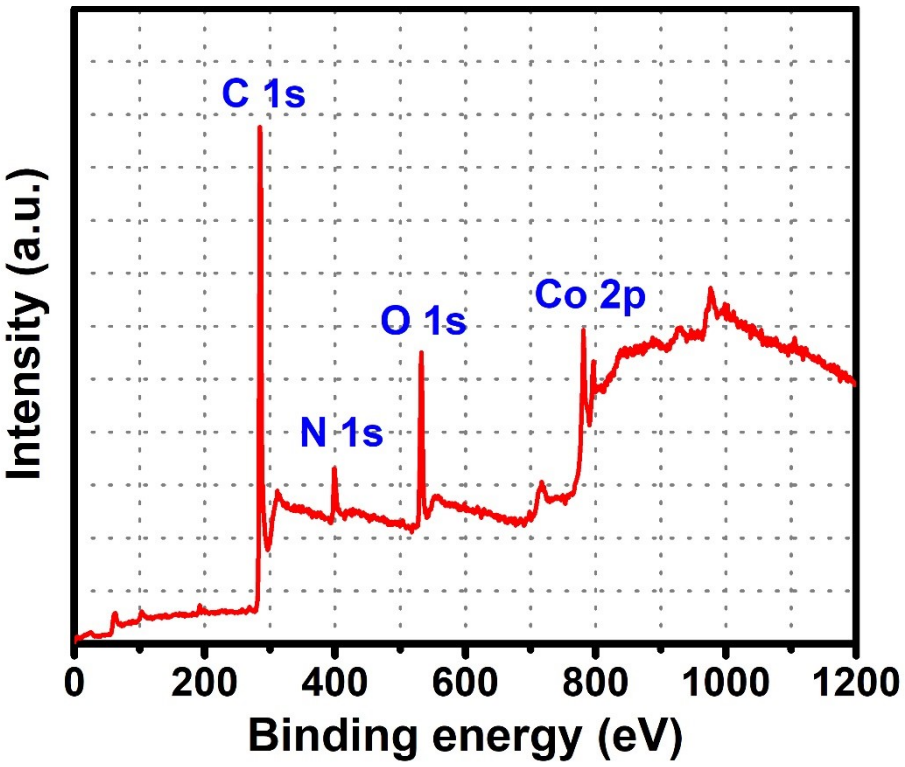

Figure S9. XPS survey scan of Co@HNCs (600) catalyst.

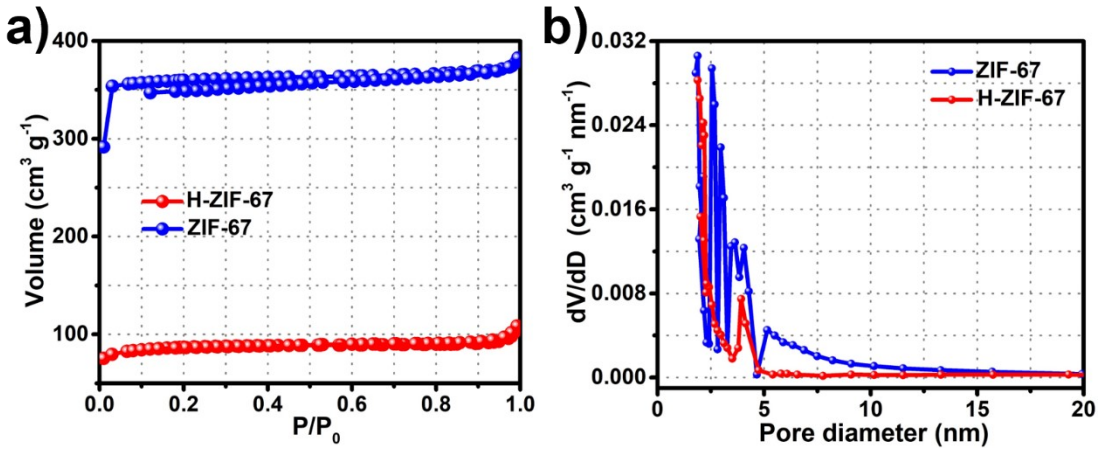

Figure S10. (a) N_2 adsorption–desorption isotherms and (b) the corresponding pore distribution of ZIF-67 and H-ZIF-67 samples.

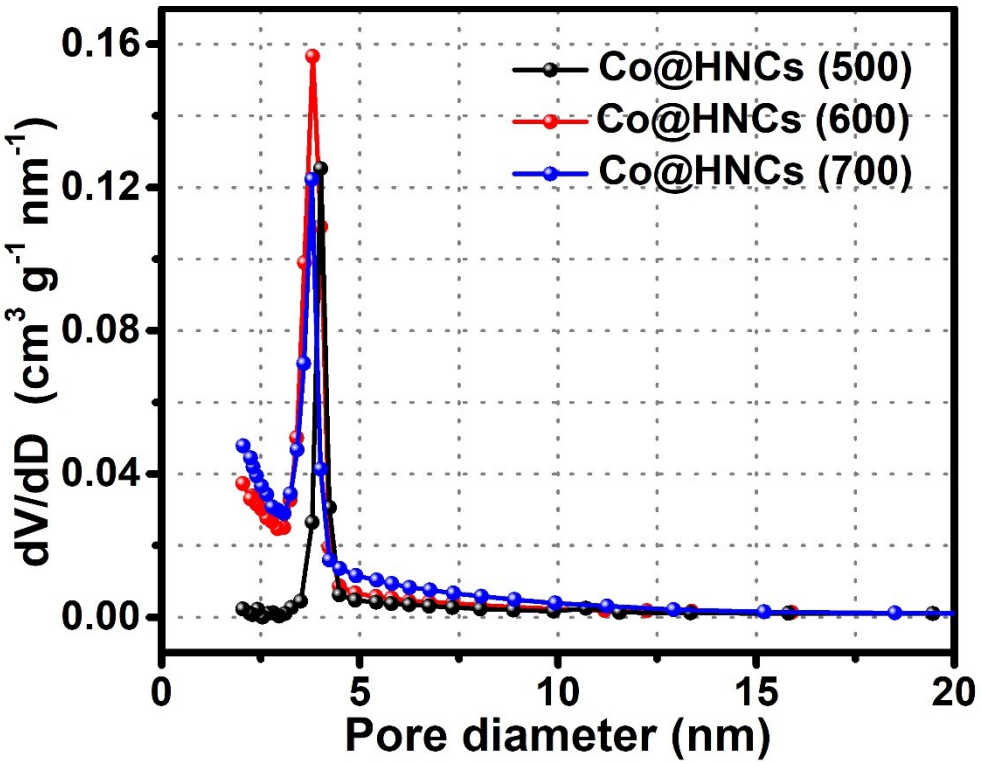

Figure S11. The corresponding pore distribution of Co@HNCs (500), Co@HNCs (600) and Co@HNCs (700) catalyst.

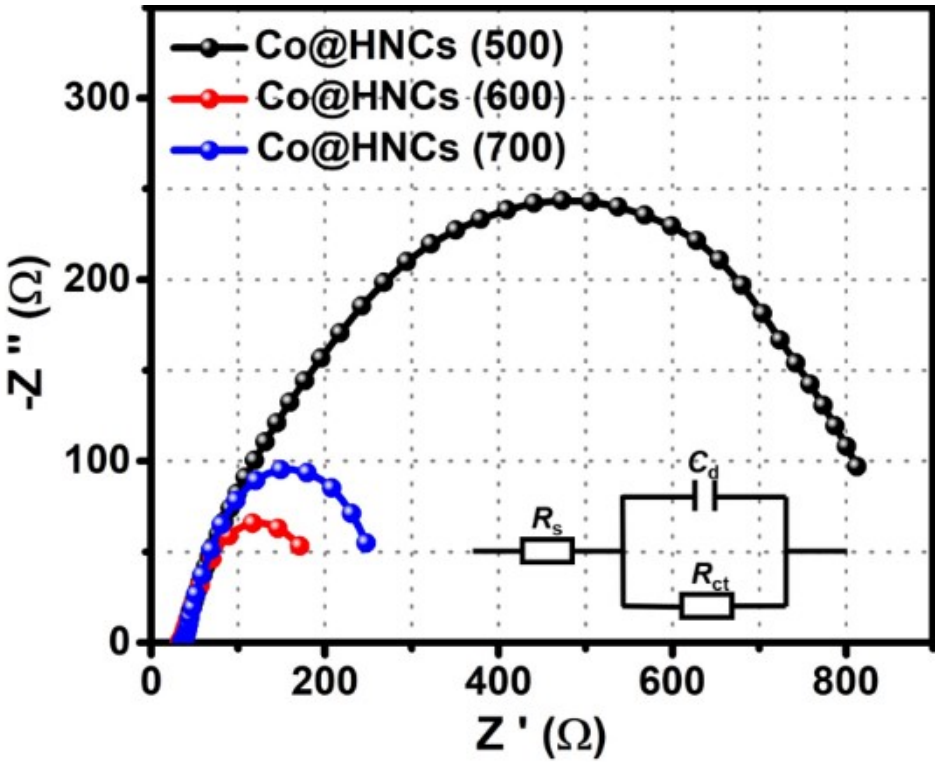

Figure S12. Electrochemical impedance spectroscopy (EIS) plots of Co@HNCs (500), Co@HNCs (600), Co@HNCs (700) electrodes at 0.87 V (vs. RHE) for ORR and the equivalent circuit (R_s: ohm resistance, R_{ct}: charge transfer resistance, C_d: capacity)

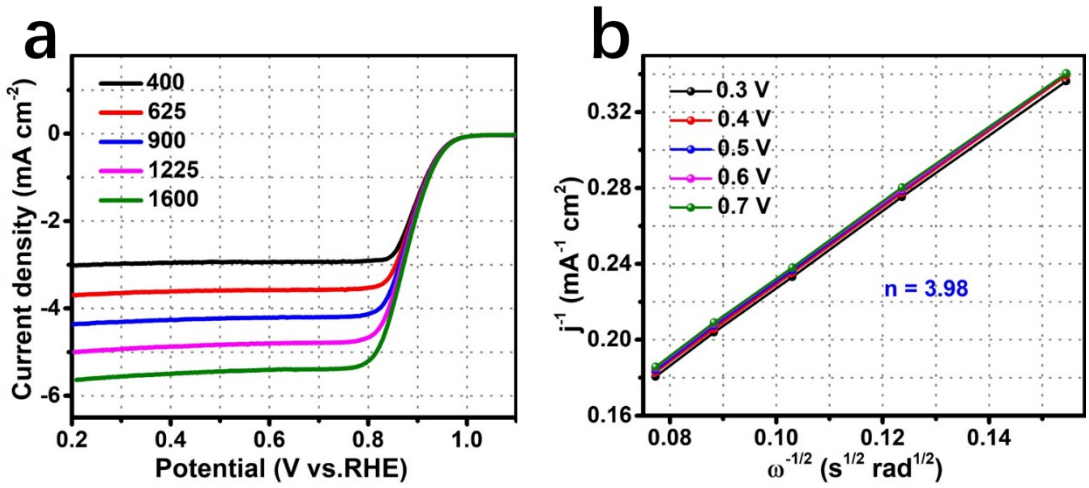

Figure S13. (a) LSV at different rotating speed in O_2-saturated 0.1 M KOH solution of Co@HNCs (600) and (b) The corresponding Koutecky-Levich (K-L) plots of j^{-1} vs $\omega^{-1/2}$ at different potentials derived from the LSV data.

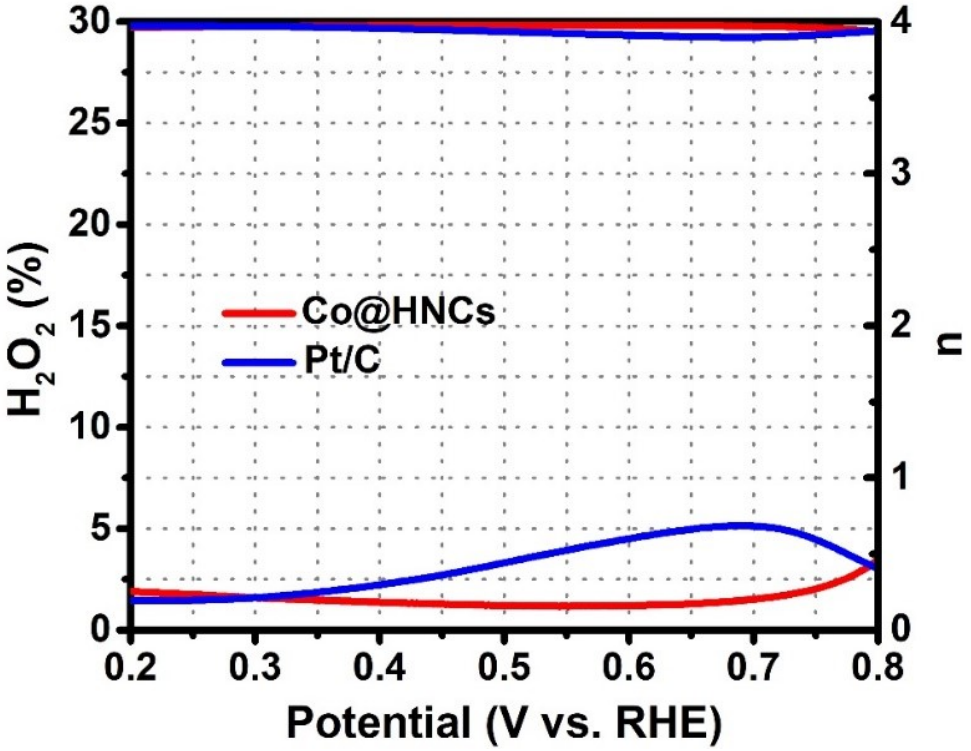

Figure S14. H_2O_2 yield and electron transfer number for Co@HNCs (600) and Pt/C sample.

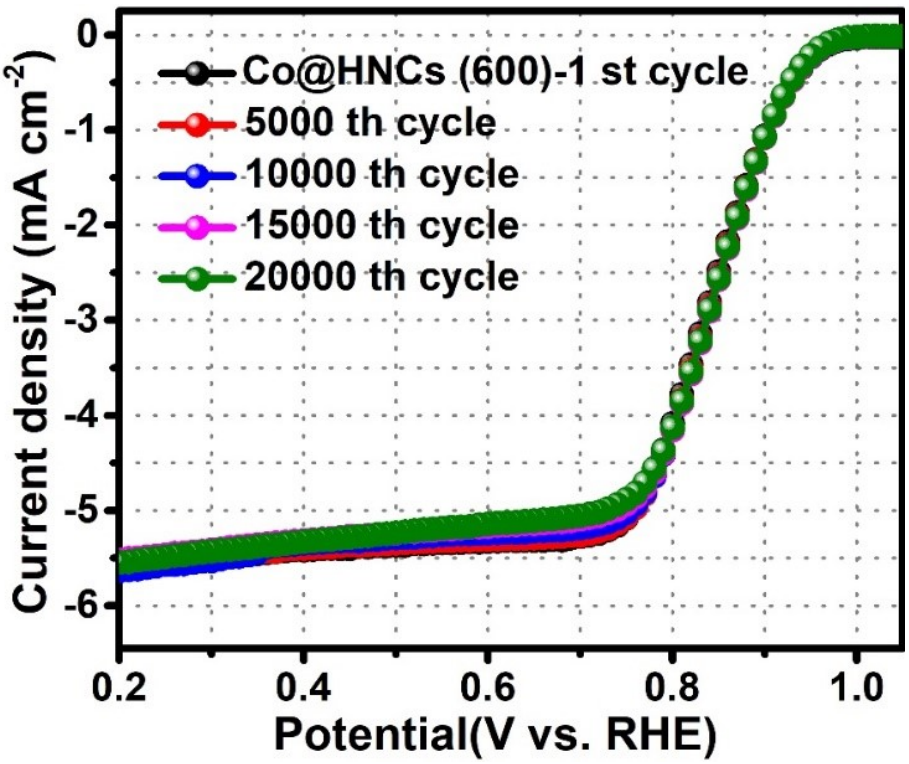

Figure S15. LSV curves for Co@HNCs (600) sample before and after 20000 cycles.

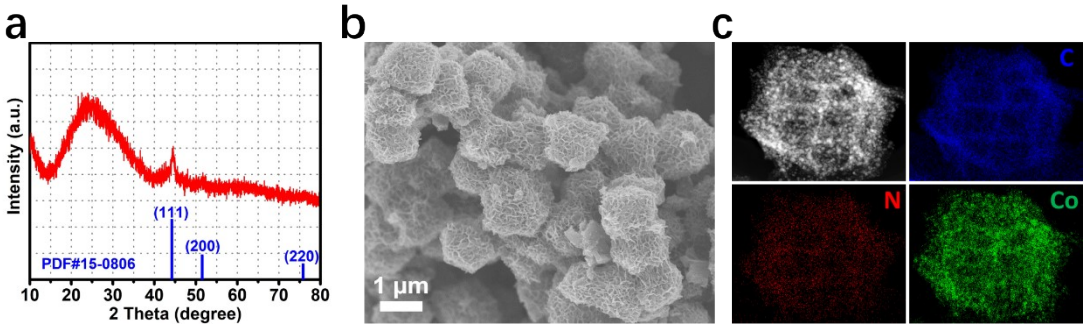

Figure S16. (a) XRD pattern, (b)SEM image, (c)and element mapping of Co@HNCs (600) after ORR

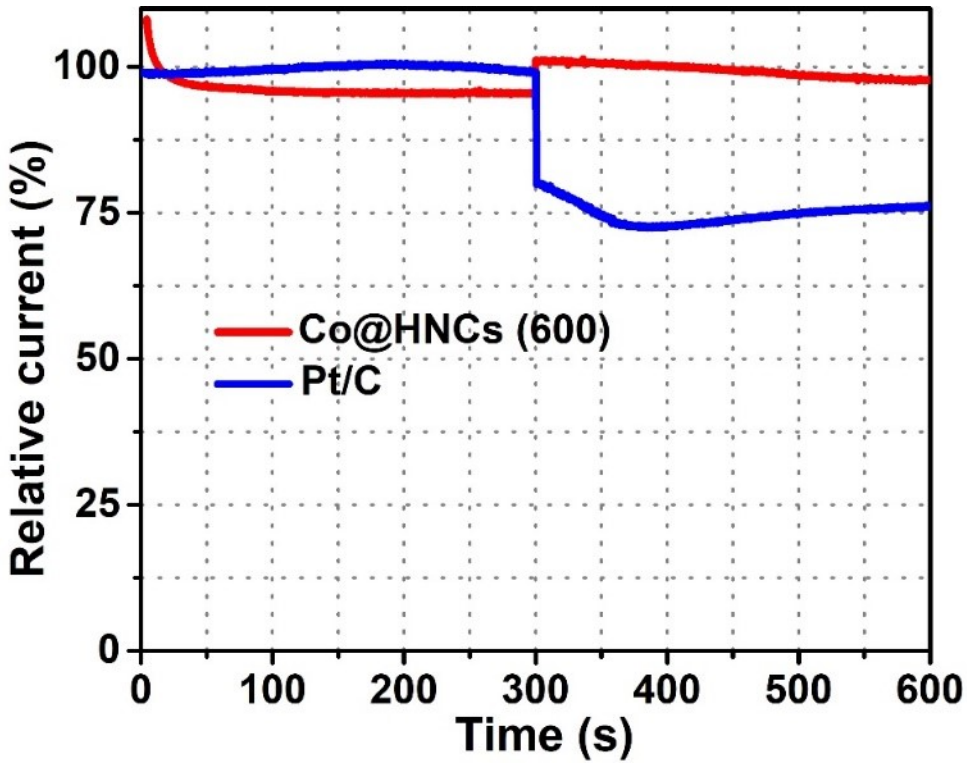

Figure S17. Methanol crossover resistance test of Co@HNCs (600) and Pt/C catalysts.

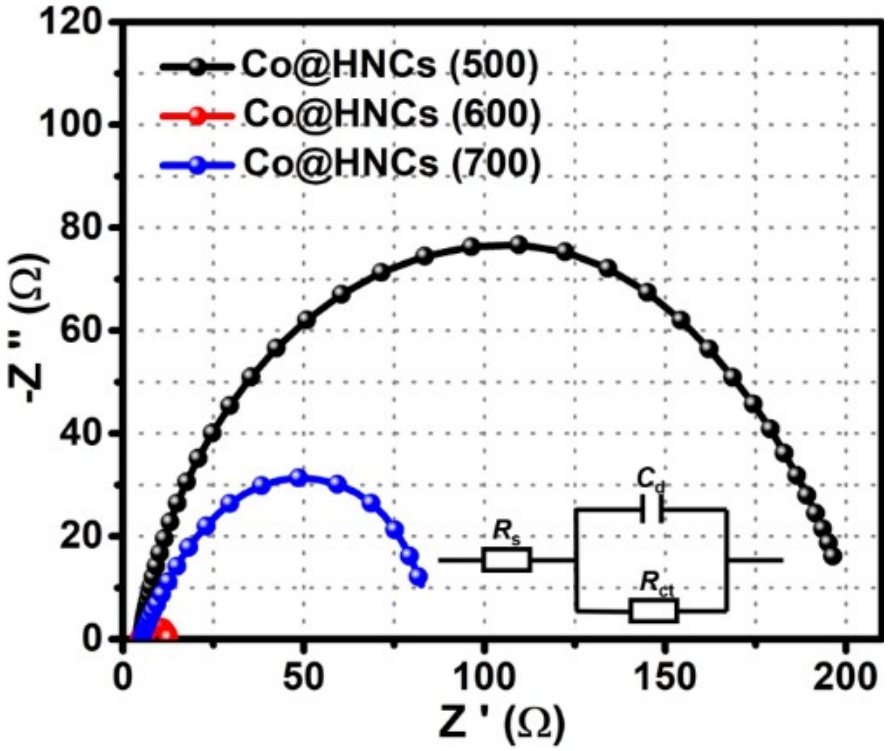

Figure S18. Electrochemical impedance spectroscopy (EIS) plots of Co@HNCs (500), Co@HNCs (600), Co@HNCs (700) electrodes at 1.6 V (vs. RHE) for OER and the equivalent circuit (R_s: ohm resistance, R_{ct}: charge transfer resistance, C_d: capacity)

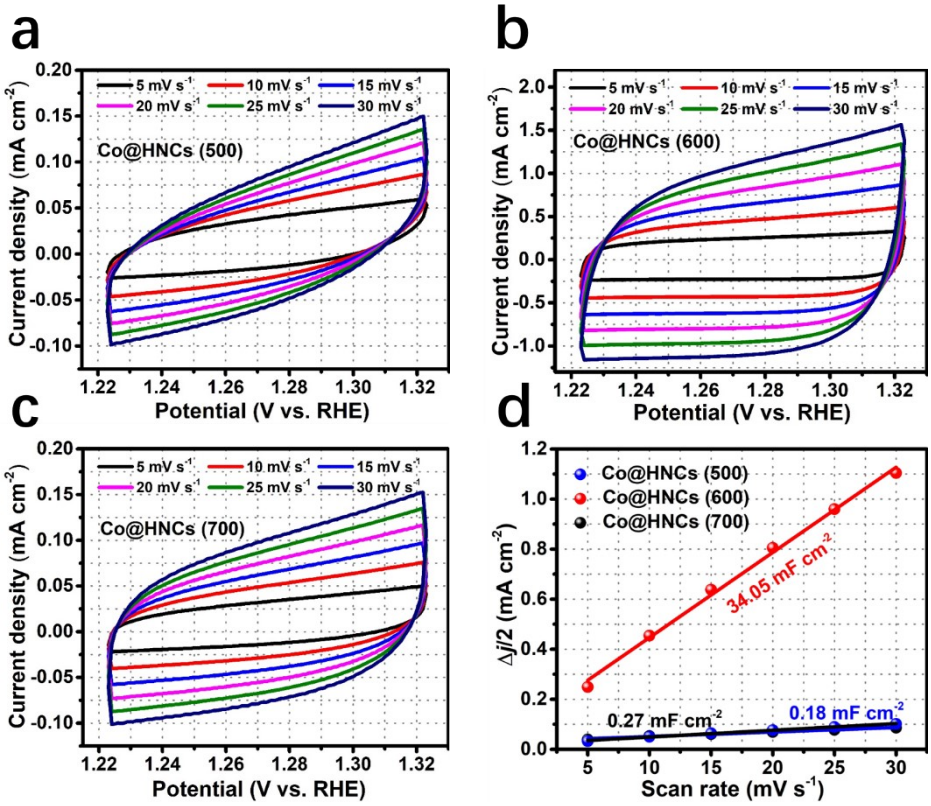

Figure S19. Cyclic voltammograms curves for (a) Co@HNCs (500), (b) Co@HNCs

(600) and (c) Co@HNCs (700) in the region of 1.223 ~1.323 V vs. RHE at various scan rates. (d) The differences in current density variation ($\Delta j = j_a - j_c$) at the potential of 1.273 V vs. RHE plotted against scan rate fitted to estimate the electrochemical double-layer capacitances (C_{dl}).

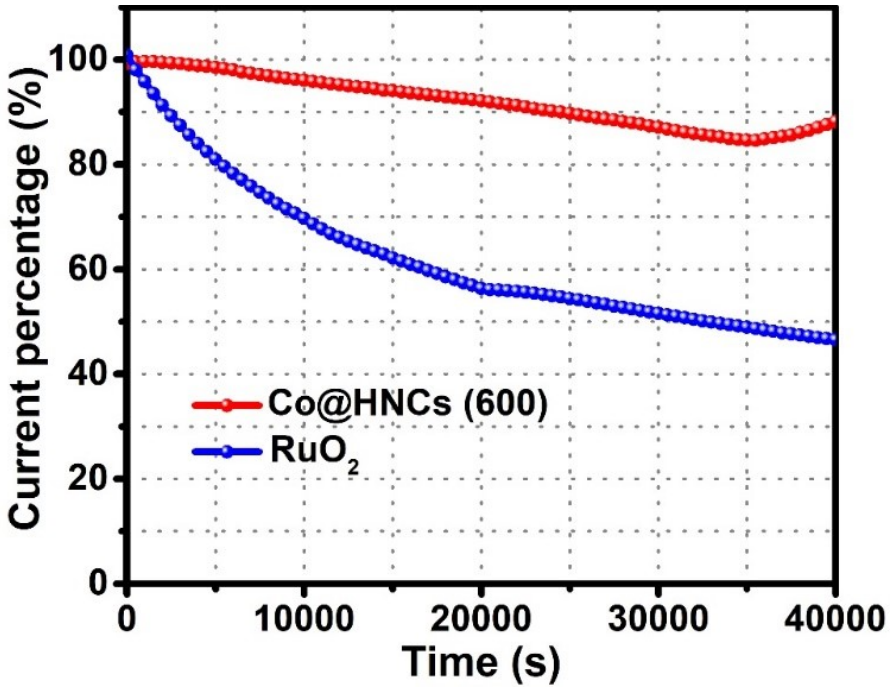

Figure S20. OER endurance test of Co@HNCs (600) catalyst in 1 M KOH.

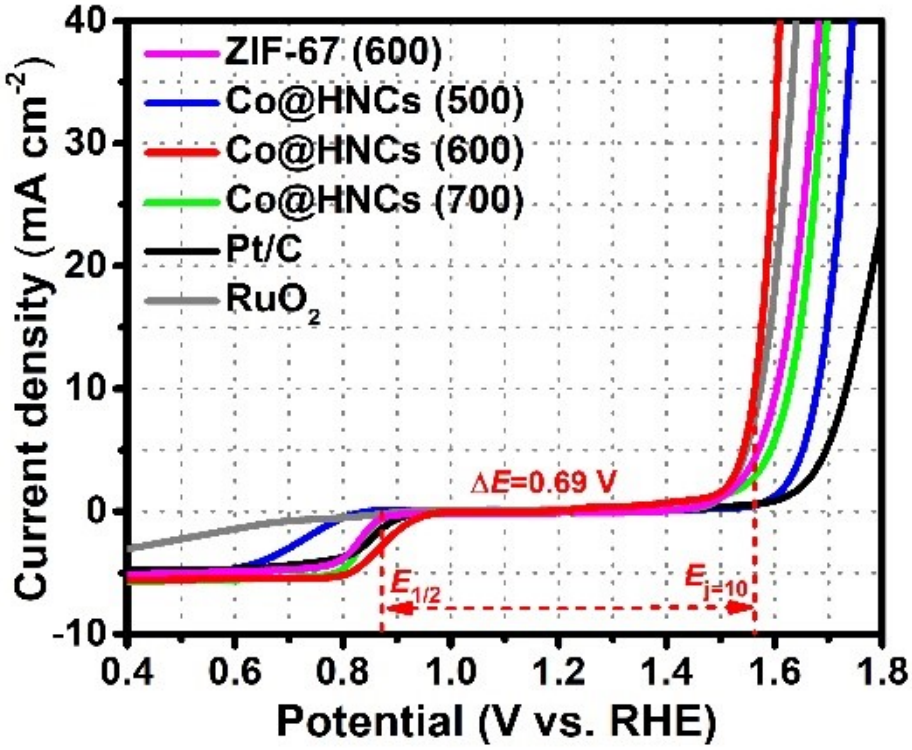

Figure S21. Bifunctional polarization profiles for various catalysts.

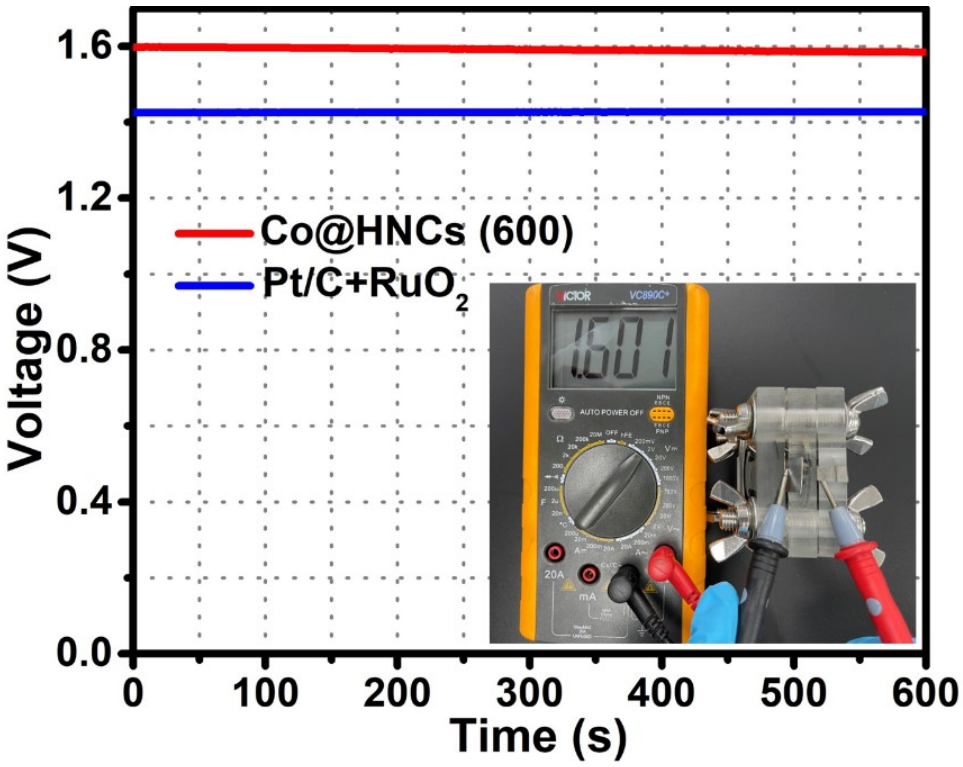

Figure S22. Open-circuit plots of Zn−air batteries using Co@HNCs (600) and commercial Pt/C+RuO_2 as the cathodic catalysts (insert shows the visual photographic image of OCV of Co@HNCs (600)-based Zn−air battery).

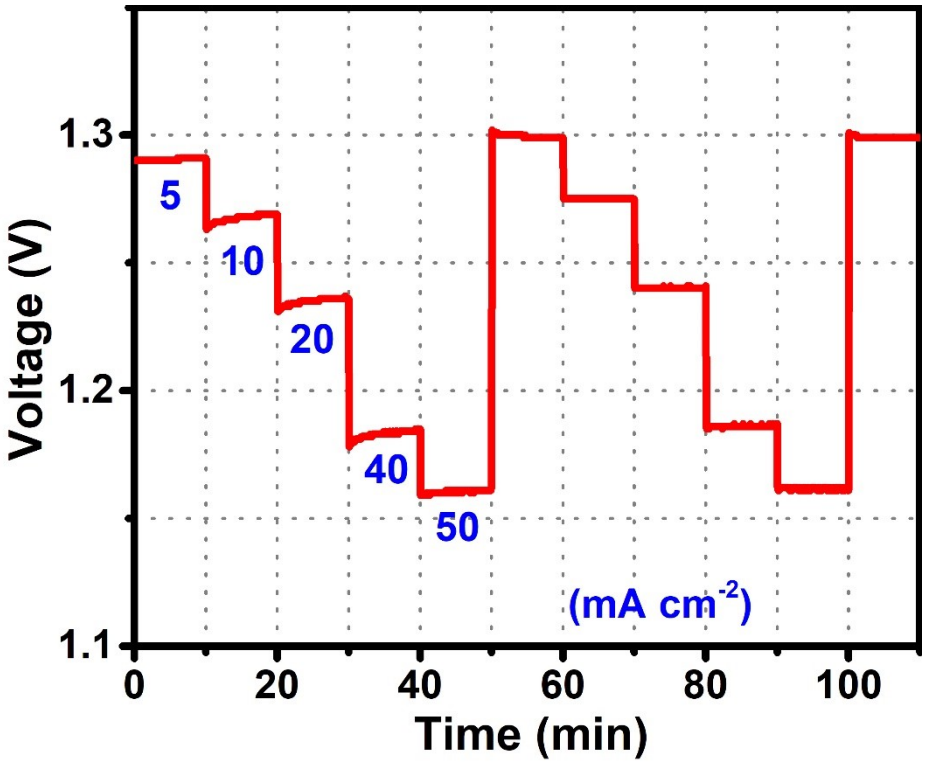

Figure S23. Galvanostatic discharge curves of the primary Zn−air batteries with

Co@HNCs (600) as cathode catalysts at different current densities.

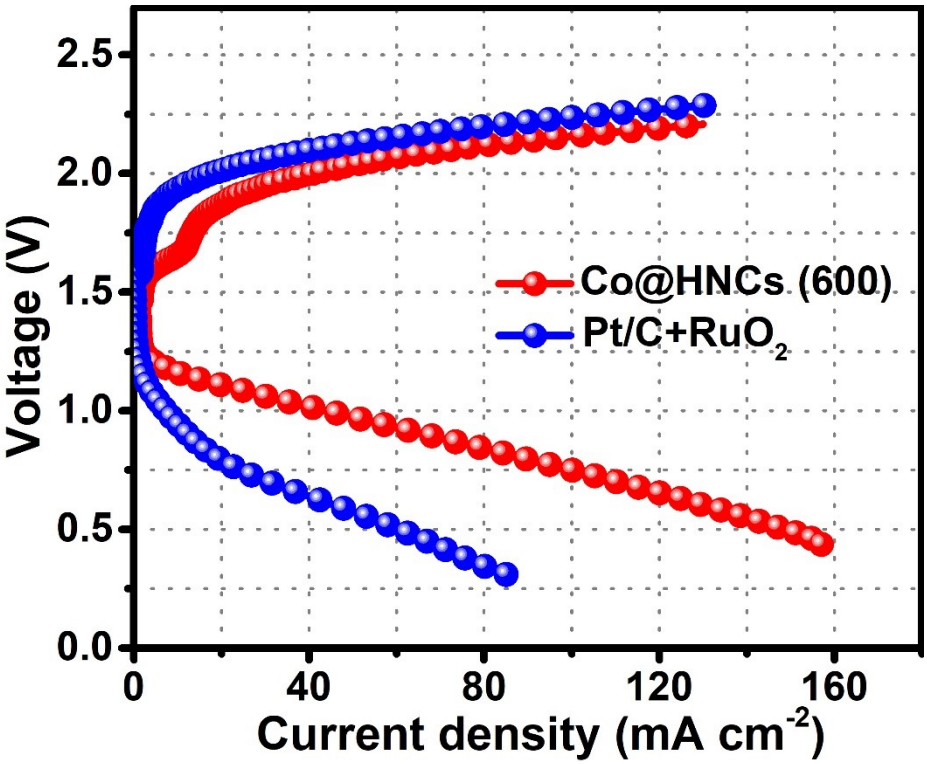

Figure S24. Polarization curves of Zn-air batteries based on as-prepared catalysts and commercial Pt/C+RuO_2 catalyst.

Table S1. The Comparison of ORR performance of non-precious Co@HNCs(600) catalysts from the recent literature and this work (0.1 M KOH medium).

Catalysts	Half-wave potential	Onset potential (V vs. RHE)	Electron transfer numbers	Reference
Co@HNCs (600)	**0.87**	**0.98**	**3.98**	**This work**
Co SA+Co_9S_8/HCNT	0.855 V	0.90 V	3.99	Small, 2020, 16, 1906735.
Co-Co_3O_4@NAC	0.795	0.935	3.8	Appl. Catal. B, 2020, 260, 118188.
Co-pyridinic N-C	0.87	0.99	3.88-3.99	Adv. Energy Mater., 2020, 10, 2002592.
Zn/CoN-C	0.861	1.004	3.88	Angew. Chem. Int. Ed., 2019, 58, 2622 –2626.
Co-SAs@NC	0.82	0.96	3.9	Angew. Chem. Int. Ed., 2019, 58,

				5359-5364.
Co-N-C- 900	0.87	0.928	3.70-3.93	Adv. Energy Mater., 2018, 8, 1801956.
NC-Co SA	0.87	1.0	4.07	ACS Catal., 2018, 8, 8961−8969.
Co SAs/PTF	0.808 V	0.89 V	3.92–3.97	J. Mater. Chem. A, 2019, 7, 1252–1259.
CoN_4/NG	0.87 V	0.96 V	3.92-4.0	Nano Energy, 2018, 50, 691–698.
Co@MCM	0.78 V	0.95 V	3.7	Energy Environ. Sci., 2018, 11, 1980–1984.
A-Co@ CMK-3-D	0.835 V	0.946 V	3.9	Small Methods, 2019, 3, 1800450.
Co-ISAS/p-CN	0.838 V	0.92 V	3.9	Adv. Mater., 2018, 30, 1706508.
Co-POC	0.83 V	0.90 V	3.6	Adv. Mater., 2019, 31, 1900592.
Co−N/CNFs	0.82	0.92	3.4	ACS Catal., 2017, 7, 6864–6871.
N-CNTs-650	0.85	0.94	3.93	J. Am. Chem. Soc., 2017, 139, 8212–8221.
Fe-N/P-C-700	0.867	0.941	3.94	J. Am. Chem. Soc., 2020, 142, 2404–2412.

Table S2. The Comparison of OER performance of non-precious Co@HNCs (600) catalysts from the recent literature and this work (1 M KOH medium).

Catalysts	**η@10 mA/cm^2 (mV)**	**Tafel slop (mV/ dec)**	**Reference**
Co@HNCs (600)	**344**	**88**	**This work**
Co-Co_3O_4@NAC	380	NA	Appl. Catal. B, 2020, 260, 118188.
Co-N,B-CSs	430	NA	ACS Nano, 2018, 12, 1894−1901.
Co_3O_4/HNCP-40	333	69.0	ACS Catal., 2018, 8, 7879−7888.

CoCePi	374	75.0	Small, 2018, 14, 1704403.
CoNiPi	402	87.0	Small, 2018, 14, 1704403.
$NiCo_2O_4$@MnO_2-CNTs	400	92	Nanoscale, 2018, 10, 13626.
NMC/Co@CNTs	500	79	Langmuir, 2018, 34, 1992−1998.
FeS/Fe_3C@N-S-C-800	570	81	Adv. Funct. Mater., 2018, 28, 1803973.
FeNi-COP-800	400	91	Appl. Catal. B, 2019, 243, 204−211.

η = Overpotential; NA = not attained.